Journal of Applied Physics

Indium surfactant assisted epitaxy of non-polar $(10\bar{1}0)$ AlGaN/InGaN multiple quantum well heterostructures

Cite as: J. Appl. Phys. **128**, 115701 (2020); https://doi.org/10.1063/5.0020263
Submitted: 29 June 2020 . Accepted: 03 September 2020 . Published Online: 16 September 2020

Brandon Dzuba, Alexander Senichev, Trang Nguyen, Yang Cao, Rosa E. Diaz, Michael J. Manfra, and Oana Malis

Journal of Applied Physics ARTICLE scitation.org/journal/jap

Indium surfactant assisted epitaxy of non-polar ($10\bar{1}0$) AlGaN/InGaN multiple quantum well heterostructures

Cite as: J. Appl. Phys. **128**, 115701 (2020); doi: 10.1063/5.0020263
Submitted: 29 June 2020 · Accepted: 3 September 2020 ·
Published Online: 16 September 2020

Brandon Dzuba,[1,2] Alexander Senichev,[1,2] Trang Nguyen,[1] Yang Cao,[1] Rosa E. Diaz,[2] Michael J. Manfra,[1,2,3,4] and Oana Malis[1,2,a)]

AFFILIATIONS

[1]Department of Physics and Astronomy, Purdue University, West Lafayette, Indiana 47907, USA
[2]Birck Nanotechnology Center, West Lafayette, Indiana 47907, USA
[3]School of Electrical and Computer Engineering, Purdue University, West Lafayette, Indiana 47907, USA
[4]School of Materials Engineering, Purdue University, West Lafayette, Indiana 47907, USA

[a)]**Author to whom correspondence should be addressed:** omalis@purdue.edu

ABSTRACT

The use of an indium surfactant considerably alters the composition and morphology of low-temperature non-polar m-plane ($10\bar{1}0$) $Al_xGa_{1-x}N$ ($x \sim 0.2$) and of silicon-doped AlGaN/InGaN multiple quantum wells grown by plasma-assisted molecular beam epitaxy. This paper compares heterostructures grown with indium surfactant with those grown under conventional stoichiometric and gallium-rich conditions at the relatively low temperature necessary for growth of $In_{0.16}Ga_{0.84}N$ quantum wells (565 °C). Stoichiometric growth results in rough, inhomogeneous AlGaN layers that are unsuitable for optical devices. Gallium-rich growth produces a smoother AlGaN layer, reduced inhomogeneities, and sharper interfaces as compared to stoichiometric growth. However, due to the low temperature, gallium-rich growth leads to the formation of an unintentional GaN layer on top of each AlGaN barrier, reducing the energies of confined electronic states in the quantum wells. An indium surfactant enables two-dimensional AlGaN growth at low temperature, producing atomically flat surface morphology and sharp heterostructure interfaces. Indium surfactant assisted epitaxy also eliminates the high aluminum alloy inhomogeneities observed with conventional stoichiometric and gallium-rich growth. Even though partial indium incorporation into the AlGaN layer is found at the studied temperatures, the high-quality, uniform non-polar $In_{0.055}Al_{0.19}Ga_{0.755}N/In_{0.16}Ga_{0.84}N$ quantum wells grown with indium surfactant display bright and narrow photoluminescence that is essential for device applications.

I. INTRODUCTION

III-nitride materials have long been proven to be an outstanding platform for the development of visible and ultraviolet optoelectronic devices such as light emitting diodes (LEDs) and laser diodes (LDs).[1–4] More recently, III-nitrides have been investigated for infrared emitters and detectors.[1,5–10] This is primarily due to their large conduction band offset (CBO) and sub-picosecond intersubband (ISB) relaxation.[1] The large CBO attainable in III-nitride heterostructures allows ISB energy in the near-infrared (NIR) range that is not accessible with arsenide and phosphide materials.[1] The primary focus of previous works in the III-nitride material system was mostly on structures grown on polar c-plane-oriented GaN that resulted in the realization of various optoelectronic devices. However, the development of ISB devices on c-plane GaN substrates is hindered by the spontaneous and piezoelectric polarization fields associated with the lack of inversion symmetry.[11] Strong polarization fields alter the conduction band of quantum well (QW) structures, resulting in lower transition energies and lower maximum confinement energies accessible for a given material combination.[5] Growth on low-defect density free-standing m-plane ($10\bar{1}0$) GaN substrates enables the study of structures without polarization fields and practical implementation in ISB devices.

AlN/GaN heterostructures provide a large conduction band offset. However, these structures are severely limited by the low critical thickness of AlN layers on GaN substrates that Lee *et al.*

reported to be ~5 nm on the c-plane.[12] While a detailed study of the critical thickness of m-plane (10$\bar{1}$0)-oriented AlN on GaN has yet to be conducted, we expect similar or more restrictive limitations due to the higher degree of strain in m-plane structures coupled with its anisotropic nature. To reduce strain, nonpolar m-plane AlGaN/GaN structures around 0.6 aluminum mole fraction can be used, as this composition results in reduced lattice mismatch while also providing sufficient CBO to confine NIR transitions. However, there have been several reports of various material homogeneity issues in non-polar AlGaN grown by plasma-assisted molecular beam epitaxy (PAMBE).[13–15] We have previously demonstrated that metal-rich AlGaN layers grown by PAMBE on m-plane GaN with large aluminum mole fractions result in intercalated planar defects of high aluminum content.[13] This is currently attributed to a changing surface morphology, where initially long step terraces promote Al–N dimer incorporation, while over time, step-bunching causes shorter step terraces that favor Ga–N dimer incorporation.[13,16] Due to this step-bunching transition, PAMBE growth of m-plane AlGaN with the aluminum composition above 0.6 is found to be unstable, hindering the realization of AlGaN/GaN heterostructures for NIR transitions.

An alternative path to increasing the CBO of these structures without increasing the aluminum mole fraction above the critical value, and hence preserving the AlGaN material homogeneity, is by introducing indium into the quantum well to grow AlGaN/InGaN heterostructures. Fireman *et al.* demonstrated the growth of low indium-content strain compensated $Al_{0.25}Ga_{0.75}N/In_{0.09}Ga_{0.91}N$ films at the temperature of 620 °C without defects or material inhomogeneities apparent in either cathodoluminescence or atom probe tomography.[17] Simulation of AlGaN/InGaN heterostructures using a self-consistent Schrödinger–Poisson solver suggests that the CBO sufficient for NIR transitions can be achieved with aluminum and indium compositions of 20% and 16%, respectively.[18] We have recently demonstrated the growth of high-quality m-plane InGaN with up to 0.16 indium molar fraction.[19] To obtain 0.16 indium molar fraction in InGaN quantum wells, the entire AlGaN/InGaN structure must be grown at low temperature, near 565 °C. To our knowledge, the epitaxy and structural characteristics of non-polar AlGaN films grown at these low temperatures have not yet been reported.

Similar to GaN, AlGaN is optimally grown at high temperature under gallium-rich conditions to enhance the mobility of surface adatoms.[20] At low temperature, though, excess gallium cannot be thermally desorbed from the surface, resulting in the formation of an unintentional GaN layer on top of the AlGaN layer. Alternatively, AlGaN can be grown with an indium surfactant, which has been shown through metal organic chemical vapor deposition (MOCVD) and MBE on various surface orientations at high temperature to reduce inhomogeneities,[21] decrease the density of certain defects,[22,23] and promote two-dimensional growth.[24,25] In this work, we demonstrate the growth of AlGaN/InGaN multiple quantum well (MQW) structures by PAMBE and compare material quality of low-temperature AlGaN grown under stoichiometric conditions, gallium-rich conditions, and by employing indium as a surfactant material. We find that while both gallium-rich and indium surfactant growth methods result in smooth surfaces at low temperature, the indium surfactant growth method yields atomically flat surfaces. High resolution scanning transmission electron microscopy (HR-STEM) images reveal aluminum fluctuations in AlGaN layers grown by stoichiometric and gallium-rich growth conditions. These inhomogeneities were not found in AlGaN grown under an indium surfactant. The indium surfactant sample exhibits narrower photoluminescence (PL) linewidth at both room temperature and liquid nitrogen temperature, most likely indicating improved heterointerface quality. The improved material quality observed in low-temperature m-plane AlGaN grown under an indium surfactant makes promising the realization of NIR ISB structures.

II. EXPERIMENTAL

All structures were grown by PAMBE in a system equipped with conventional effusion cells for aluminum, indium, gallium, and silicon (see also the supplementary material for details of the growth procedures). Atomic nitrogen was supplied to the substrate using a Veeco Unibulb radio frequency (RF) plasma source. All growths were done on m-plane (10$\bar{1}$0) GaN substrates gallium-mounted to c-plane 2-in. GaN/Sapphire host wafers. The commercially available (10$\bar{1}$0) free-standing GaN substrates were purchased from Nanowin Science and Technologies Company. These substrates have a threading dislocation density $<5\times10^{6}$ cm^{-2}, a miscut of $-0.5°\pm0.2°$ toward the (0001) direction, and an initial root mean squared (RMS) roughness <0.3 nm over a $4\times4\,\mu m^2$ area. Prior to growth, the substrates were prepared by sonication in trichloroethylene (TCE), acetone, and methanol, rinsed with de-ionized water, and dried with N_2 gas. The substrates were then loaded into an ultrahigh vacuum (UHV) chamber and outgassed at ~500 °C for >12 h. They were then loaded into the MBE chamber, where a 150 nm thick GaN buffer layer was grown at 720 °C under gallium-rich conditions. All excess gallium metal was either desorbed or consumed by nitrogen at the end of the buffer growth. Control samples show that the resulting buffer layer grown under these conditions is free of droplets with a surface that shows pronounced step terraces and undulations characteristic of (10$\bar{1}$0) GaN grown on c-miscut m-plane substrates[26] as measured by atomic force microscopy (AFM).

The active nitrogen flux for a N_2 flow rate of 0.5 sccm and RF power of 300 W was measured to be 5.8×10^{14} atoms/cm^2 s. This was calibrated by transmission electron microscopy measurements of the thickness of a GaN layer grown under nitrogen-limited conditions on m-plane GaN substrates. For the growth of m-plane $Al_{0.20}Ga_{0.80}N$ barriers, the active nitrogen flux was estimated by growing an AlGaN film in the nitrogen-limited regime at low temperature, below the onset of thermal desorption of gallium and decomposition of GaN. The thickness and composition of this layer were determined by modeling x-ray diffraction (XRD) symmetric ω–2θ scans, and the resulting active nitrogen flux was found to be $\sim5.4\times10^{14}$ atoms/cm^2 s, smaller than determined by GaN growth for the same plasma conditions. The decrease in the available nitrogen flux for AlGaN layers relative to GaN layers is likely due to the suppression of Ga–N dimer incorporation and subsequent nitrogen loss from the growth front, as we have previously reported.[13] The active nitrogen flux determined through the growth of low-temperature AlGaN is referred in this work as the effective nitrogen flux Φ_N^{eff} and is used to define a III/V ratio for the growth of AlGaN barriers.

The aluminum flux was also calibrated through the growth of 40 nm thick m-plane $Al_{0.20}Ga_{0.80}N$, whose thickness and compositions were determined by XRD ω–2θ scans. The gallium flux was calibrated through the growth of 40 nm thick m-plane $In_{0.09}Ga_{0.91}N$ bulk layers at the temperature below Ga thermal desorption, with thicknesses and compositions determined by XRD symmetric ω–2θ scans. Finally, the indium flux was calibrated through the growth of a thick c-plane InN film, grown below 450 °C, where indium desorption is negligible.[27]

Due to the relatively low flux needed for doping, the silicon cell cannot be calibrated in the same manner as the metal sources. Thus, a continuously doped c-plane InAlN sample was characterized with secondary ion mass spectroscopy (SIMS) measurements at EAG Laboratories. The measured silicon concentration in this sample was 7.69×10^{20} cm^{-3} at an InAlN growth rate of 0.9 nm/min, yielding a silicon flux of 1.15×10^{12} atoms/cm^2 s. For all heterostructures in this study, silicon was deposited during two 10-s growth interruptions resulting in a silicon sheet density of 1.15×10^{13} cm^{-2} (δ-doping) located 1 nm away from each interface in the AlGaN barriers.

Growth conditions in which the supplied metal flux, $\Phi_{Ga} + \Phi_{Al}$, is approximately equal to the effective active nitrogen flux, Φ_N^{eff}, are defined as stoichiometric. These conditions were experimentally determined by observing the reflection high-energy electron diffraction (RHEED) intensity recovery times for $Al_{0.20}Ga_{0.80}N$ layers grown under varying gallium fluxes. At low metal fluxes, the recovery time is nearly zero, indicating no metal adlayer on the surface. These measurements were also used to determine gallium-rich conditions, where the III/V ratio is ∼1.2 (see the supplementary material for details).

This paper focuses on three m-plane (In)AlGaN/InGaN MQW structures grown at the same temperature, 565 °C, but with different conditions during barrier growth. Each structure has 15 periods, with an additional barrier layer grown at the end of the structure. All InGaN quantum wells (QWs) are ∼2.8 nm wide with an indium composition of about 16%. The InGaN composition and growth rate were determined previously in bulk layers grown under identical conditions.[19] These QWs are grown under effectively indium-rich conditions to ensure growth underneath an indium adlayer. We previously demonstrated in 30 nm bulk InGaN layers that this growth method produces atomically flat, coherently strained material.[19] Two n-type δ-doping silicon layers were placed in each barrier ∼1 nm away from each interface, which is essential to measure ISB absorption.[28] It is worth noting that silicon is a known anti-surfactant for III-nitride materials[29,30] and is expected to reduce the mobility of surface adatoms. It has previously been reported for c-plane GaN grown by metal organic vapor phase epitaxy (MOVPE) and PAMBE that silicon concentrations above 1.9×10^{19} cm^{-3} and 2×10^{20} cm^{-3}, respectively, can cause material quality issues.[31,32] However, to our knowledge, no such effects have yet been reported for m-plane nitrides. Moreover, a silicon δ-doping technique was used in this work instead of continuous doping.

The growth conditions for the AlGaN barriers are summarized in Fig. 1. First, a stoichiometric AlGaN structure was grown such that the aluminum and gallium fluxes were approximately equal to the active effective nitrogen flux. Then, a gallium-rich

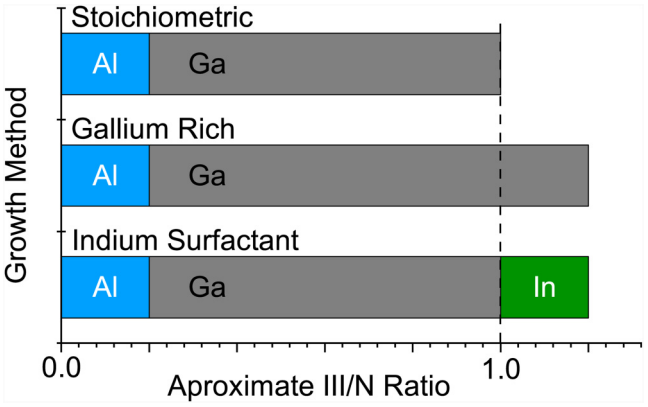

FIG. 1. Schematic representation of the metal fluxes used in AlGaN barriers. Each layer was grown with an effective active nitrogen flux of 5.4×10^{14} atoms/cm^2 s and an aluminum flux of $\sim 1.1 \times 10^{14}$ atoms/cm^2 s. The indium flux level represents the average indium flux provided during the barrier growth. The growth temperature for all structures was 565 °C ± 4 °C as measured by a pyrometer.

structure was grown with a III/V ratio of ∼1.2. All gallium remaining on the surface after the growth of each barrier was consumed by nitrogen, resulting in the growth of an unintentional GaN interlayer (see also the supplementary material). Finally, an indium surfactant sample was grown with aluminum and gallium fluxes similar to the stoichiometric structure, but indium was also supplied to generate growth under an indium adlayer. The amount of indium supplied to the surface was controlled through periodic indium flux interruption and thermal desorption. More details about the MBE growth procedures are given in the supplementary material. Optical microscopy images show the resulting structure had a small density of indium droplets on the surface, indicating the growth was conducted with sufficient levels of indium to assume full surface coverage.

HR-STEM was performed on all structures. Samples for high-angle annular dark-field STEM (HAADF-STEM) acquisition were prepared with a Thermo Scientific Helios G4 UX Dual Beam using the focused ion beam (FIB) *in situ* lift-out method. Lamellas were polished at 500 V and plasma cleaned to reduce the area damaged and contaminated by the high-energy ion beam. HR-STEM images were taken using a double aberration-corrected Thermo Scientific Themis Z TEM/STEM at 300 kV acceleration voltage and 0.23 nA current. These HR-STEM images were used to measure the well and barrier thicknesses as well as to study material distribution and crystalline quality of the structures.

The ternary and quaternary alloy compositions and growth rates were determined using 30–40 nm thin films grown under similar conditions. The symmetric ω–2θ scans of the MQW structures were then modeled using these thicknesses and compositions in the software package Epitaxy 4.5a provided by Malvern PANalytical. The resulting simulated curves were in good agreement with the measured curves.

The samples were additionally characterized using atomic force microscopy to probe the surface and PL measurements for

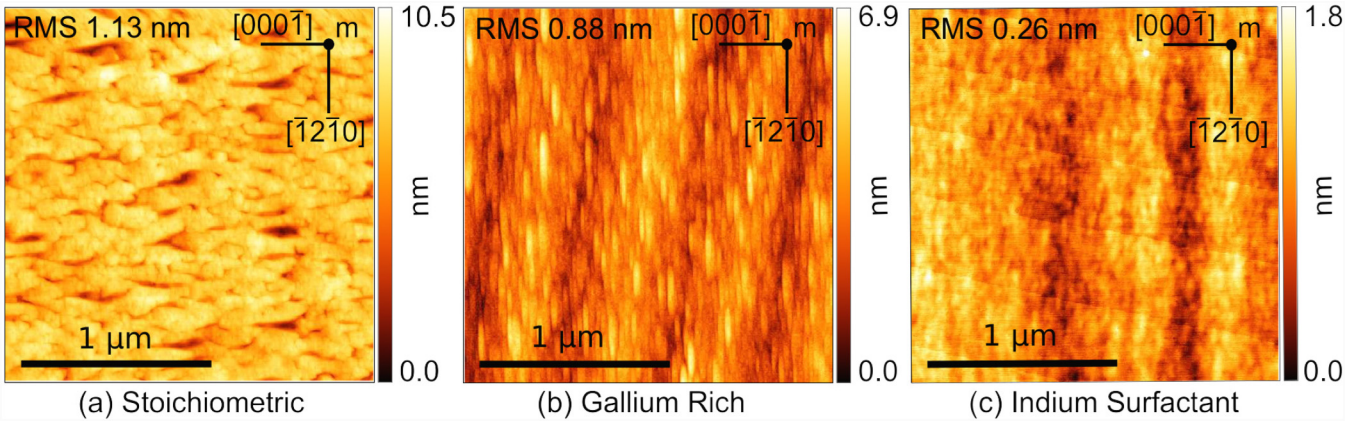

FIG. 2. $2 \times 2\,\mu m^2$ AFM images of the three MQW structures grown under (a) stoichiometric, (b) gallium-rich, and (c) indium surfactant growth conditions. The top layer of each of the structures is the final AlGaN barrier.

optical characterization. For continuous excitation PL experiments, the samples were placed in a liquid He flow cryostat and measured in reflection geometry in the range from 80 K to room temperature. Excitation power of about 10 mW (estimated cw photo-excited carrier density is 6.3×10^{11} cm^{-3}) was provided by a 325 nm cw He–Cd laser. The PL spectra were recorded with a Cary Eclipse fluorescence spectrometer equipped with a photomultiplier tube.

III. RESULTS AND DISCUSSION

Figure 2 shows the surface morphology for the three superlattice structures, each representative of the final AlGaN layer. The surface morphologies for both the stoichiometric sample and the gallium-rich sample are fairly rough, with RMS value over $2 \times 2\,\mu m^2$ of 1.13 and 0.88 nm. The indium surfactant sample, however, has an RMS roughness similar to the GaN substrate, of 0.26 nm. The rough morphology of the stoichiometric sample is most likely due to high diffusion barriers coupled with low adatom thermal energy, a result of the lack of a metal adlayer at the growth front and low growth temperature.

The surface roughness of the gallium-rich sample may indicate that the surfactant capabilities of gallium are insufficient to overcome the decreased adatom kinetic energy due to low temperature growth. The anti-surfactant properties of silicon may also contribute to surface roughness. Growth with an indium surfactant, however, appears to produce an atomically flat surface, indicating that indium may be a more desirable surfactant under these conditions. There have been several reports of surface morphology improvements through the utilization of an indium surfactant on AlGaN structures grown through MOCVD on various substrates when compared to conventional growth methods,[23,25,33] further demonstrating the surfactant capabilities of indium.

To assess the thickness of the layers, their composition, and quality of interfaces, symmetric ω–2θ scans were conducted for each sample and are presented in Fig. 3. The experimental data were compared with simulations of the XRD that assume the heterostructures are coherently strained to GaN, the QWs are 2.8 nm $In_{0.16}Ga_{0.84}N$, and the Al-composition of the barriers is the same as that of bulk AlGaN layers grown under gallium-rich conditions (see Fig. 6S in the supplementary material). While the XRD

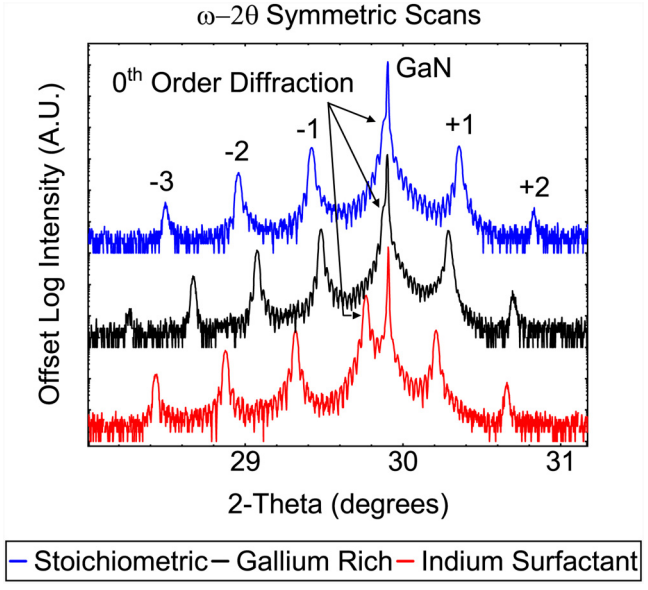

FIG. 3. Symmetric ω–2θ scans for each MQW structure grown under stoichiometric, gallium-rich, and indium surfactant growth conditions. All scans exhibit features indicative of high-quality heterostructures, such as high order satellite peaks and well-defined thickness fringes. Modeling these curves predicts the following compositions and thicknesses: (i) stoichiometric—$Al_{0.21}Ga_{0.79}N$/$In_{0.16}Ga_{0.84}N$ (7.0/2.8 nm) × 15; (ii) gallium-rich—$Al_{0.21}Ga_{0.79}N$/GaN/$In_{0.16}Ga_{0.84}N$ (7.2/1.2/2.8 nm) × 15; (iii) indium surfactant—$In_{0.055}Al_{0.19}Ga_{0.755}N$/$In_{0.16}Ga_{0.84}N$ (7.5/2.8 nm) × 15. A.U., arbitrary units.

scan for the stoichiometric superlattice shows prominent features, the intensity of the higher-order satellite peaks drops faster away from the 0th order peak than expected from simulations. This may indicate a reduction in material quality and uniformity in the MQW structure. The gallium-rich structure shows a decreased angular separation between the satellite peaks, indicating a larger period than the other structures. We attribute this result to the growth of material during the plasma pause following the AlGaN layer, where excess gallium from the AlGaN layer is incorporated into the structure in the form of an unintentional GaN layer (see also Fig. 1S in the supplementary material). This confirms the structure was indeed grown gallium-rich. Both the stoichiometric and gallium-rich structures' 0th order diffraction peaks are nearly aligned with the GaN peak, indicating that these structures are close to strain balanced.[17] In contrast, the indium surfactant sample shows a 0th order peak shifted to lower angles. As all structures have similar growth conditions for the InGaN QWs, we believe this indicates indium incorporation into the barriers of the structure.

Modeling of the ω–2θ scan of the indium surfactant structure assuming 0.19 aluminum composition indicates ∼0.055 indium molar fraction in the barriers. Additional evidence for the incorporation of indium into m-plane AlGaN at low temperature is provided by SIMS and detailed in the supplementary material (Fig. 7S). Previously published indium surfactant studies claim no significant indium incorporation into AlGaN structures using this method.[21–25,33,34] However, these studies were conducted at high temperature. At our growth temperature of 565 °C, indium removal from the growth front through thermal desorption and In–N bond dissociation is substantially reduced,[19,35] which could partially explain its incorporation into the AlGaN barrier. A detailed study of indium incorporation during AlGaN growth is beyond the scope of this work. However, early evidence indicates that some level of indium incorporation may be unavoidable at these temperatures, as it is present in gallium-rich samples when indium is also supplied (see the supplementary material). The level of indium incorporation observed in the MQW structures is in good agreement with a strain-driven incorporation model (see the supplementary material), but further study is required to confirm this hypothesis. Since indium incorporation into AlGaN barriers leads to a reduction of the CBO, the indium surfactant structure has a theoretical CBO of 442 meV, a value that is lower than the 581 meV in the structures without indium incorporation into the barrier. Therefore, with the alloy compositions reported in this paper, the indium surfactant sample is not able to support NIR ISB transitions. Further work must be done to increase the CBO of these structures to achieve NIR absorption, either through reducing the indium incorporation into the AlGaN layer or by increasing the InGaN and/or AlGaN compositions in the structure to compensate.

HR-STEM was conducted on each sample to further investigate the structural quality. Figure 4 shows a comparison between representative areas of each structure. The HR-STEM images of the stoichiometric structure [Fig. 4(a)] shows a larger gradual contrast variation between the wells and barriers; this is indicative of a rough interface or material intermixing due to atomic interdiffusion. This sample also shows several high-contrast regions in the AlGaN layer that energy dispersive x-ray analysis (EDX) confirms

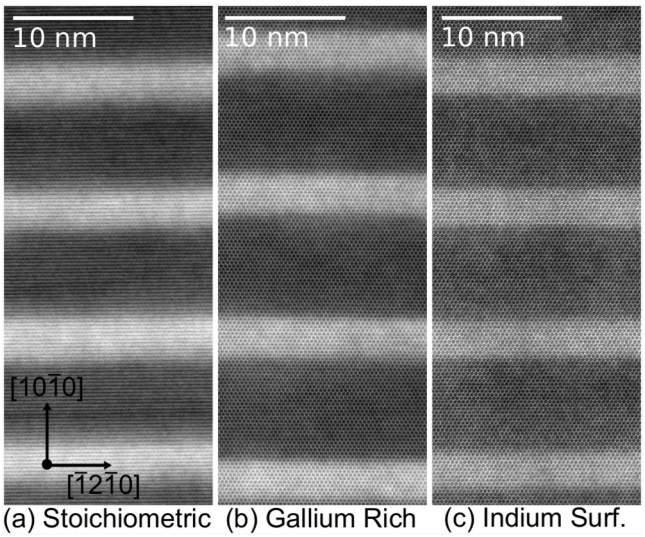

FIG. 4. Dark-field HR-STEM (0002) zone-axis images of the three structures: stoichiometric (a), gallium-rich (b), and indium surfactant (c). Here, the high brightness regions represent the InGaN well, while the darker regions represent the (In)AlGaN barriers.

are high aluminum containing inhomogeneities. The gallium-rich structure [Fig. 4(b)] shows sharper interfaces and reduced inhomogeneities, though local areas can still be found with aluminum segregation (Fig. 5). HR-STEM also confirms the larger period of the

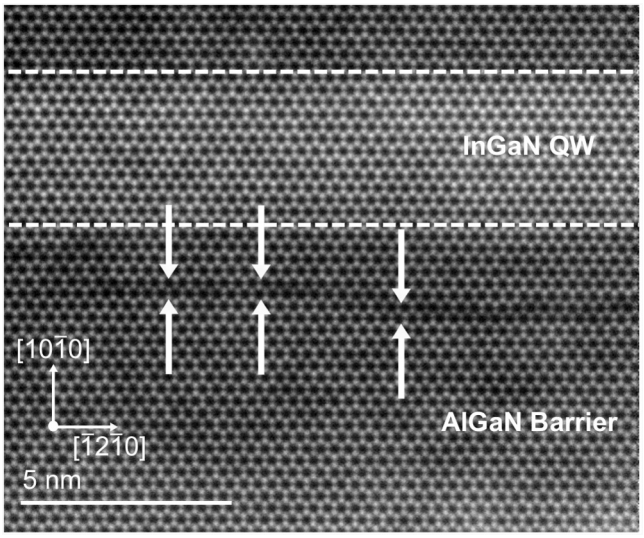

FIG. 5. Dark-field HR-STEM (0002) zone-axis image of one period of the gallium-rich structure. The dark region indicated by the white arrows represents a high aluminum containing region, confirmed by EDX measurements. These features appear periodically throughout the structure.

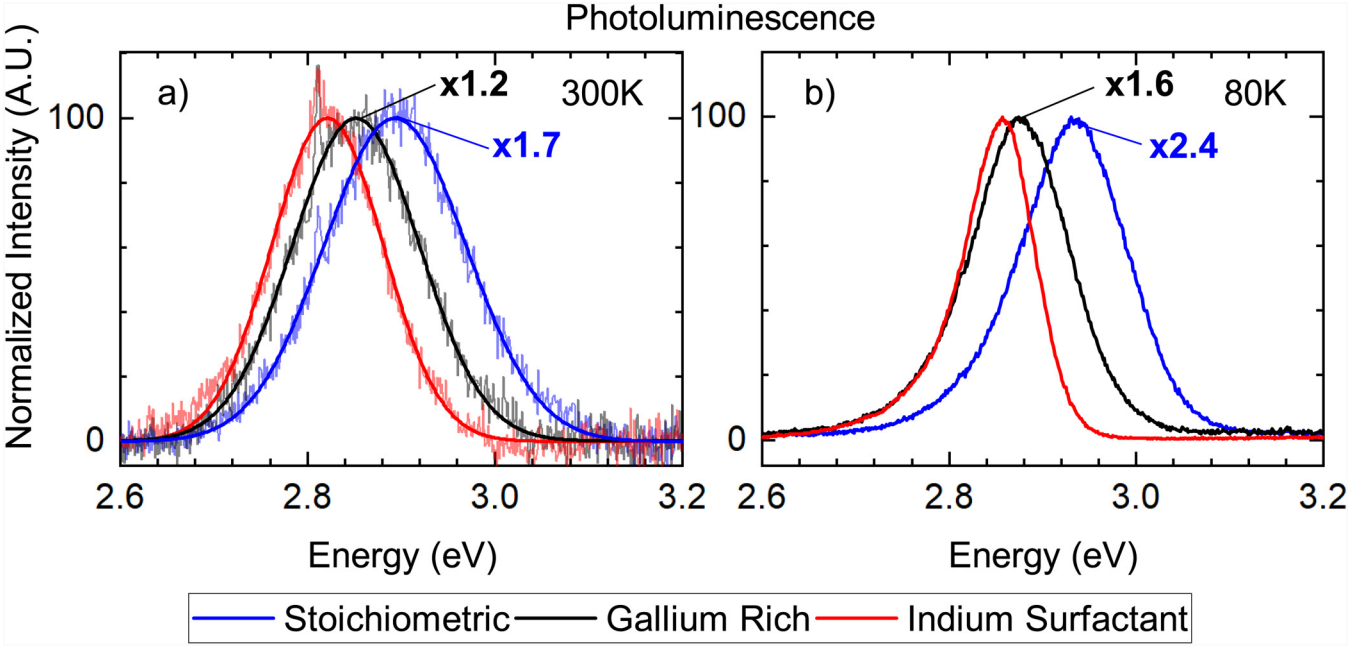

FIG. 6. Photoluminescence (PL) measurements of all structures at room temperature (a) and liquid nitrogen temperature (80 K) (b). All PL curves were scaled to reach a maximum of 100 A.U. by the factors indicated on the plots. The room temperature measurements are overlaid with a Gaussian fit as a guide for the eye due to the low signal-to-noise ratio. At 80 K, the FWHM of the spectra is 138 meV, 126 meV, and 91 meV for the stoichiometric, gallium-rich, and indium surfactant samples, respectively. At room temperature, the FWHM of the spectra is 176 meV, 160 meV, and 140 meV for the stoichiometric, gallium-rich, and indium surfactant samples, respectively. A.U., arbitrary units.

structure, where the GaN interlayer can be identified by the slower contrast change after the AlGaN layer than after the InGaN layer (see the supplementary material for details). In contrast, the indium surfactant structure [Fig. 4(c)] shows very uniform material in both the QW and barrier, and well-defined, sharp interfaces. Aluminum inhomogeneities were not observed for this sample at any length scale within the probed area. Additional larger area HR-STEM images of the samples grown gallium-rich and with indium surfactant are given in Fig. 5S in the supplementary material. These improvements are most likely due to the enhanced adatom mobility at the growth front underneath the indium adlayer. The surfactant effect of indium on AlGaN has been previously reported on c-plane (0001) structures[21,22,24,33,34] and semi-polar structures,[23,25] as well as theoretically described on c-plane (0001) by Northrup and Neugebauer.[36] However, to the authors' knowledge, this is the first demonstration of this effect on non-polar m-plane ($10\bar{1}0$) structures grown at low temperatures. These TEM results indicate that the indium surfactant growth method may alleviate the material issues found in the growth of low-temperature gallium-rich m-plane AlGaN alloys, while also eliminating the formation of a GaN interlayer.

The samples were optically characterized by photoluminescence measurements at both room temperature [Fig. 6(a)] and 80 K [Fig. 6(b)]. At 80 K, the indium surfactant sample has the narrowest linewidth, with a full-width at half-maximum (FWHM) 34% smaller than the stoichiometric sample, and 28% smaller than the gallium-rich structure. The indium surfactant structure also exhibits stronger PL intensity, with intensity 2.4 times and 1.6 times higher than the stoichiometric and gallium-rich samples, respectively. Linewidth is also reduced at room temperature, where the indium surfactant sample has a 22% reduction in linewidth compared to the stoichiometric sample and a 13% reduction when compared to the gallium-rich structure. The improvements in the PL signal at 80 K emphasize the improvement in the MQW structure when an indium surfactant is used; the reduction in the linewidth is most likely a direct result of sharper, more uniform interfaces.

IV. CONCLUSION

Three non-polar MQW (In)AlGaN/InGaN structures were grown at 565 °C on free-standing m-plane ($10\bar{1}0$) GaN substrates utilizing three different barrier growth methods: stoichiometric, gallium-rich, and indium surfactant. The stoichiometric structure showed a rough surface morphology, diffuse interfaces, broad PL signal, and severe material inhomogeneities, indicating that this growth method is not suitable for low-temperature, m-plane AlGaN growth. The gallium-rich structure showed improved material and structural quality relative to the stoichiometric structure, though high aluminum containing regions were still present at reduced density. Gallium-rich growth also leads to the formation of a GaN interlayer in the structure. The indium surfactant sample

showed the smoothest surface, sharpest interfaces, and narrowest PL linewidth, with no visible material inhomogeneities. However, using an indium surfactant during the AlGaN barrier leads to the inclusion of ∼5.5% indium into the barrier, reducing the CBO of the structure by ∼24%. Early results show that some level of indium incorporation may be unavoidable at these temperatures, and further investigation must be conducted to determine its driving mechanism. To our knowledge, this is the first demonstration of m-plane AlGaN/InGaN structures with high indium composition and the first demonstration of m-plane AlGaN/InGaN structures grown with an indium surfactant. However, future work must be conducted to increase the CBO of these structures, either through limiting the unintentional indium incorporation into the barrier or by further increasing indium and aluminum compositions in the well and barrier materials, respectively. We show here that utilizing indium as a surfactant facilitates the two-dimensional growth of homogeneous low-temperature m-plane AlGaN. We believe this technique to be a promising candidate for the future development of m-plane AlGaN/InGaN structures for device applications.

SUPPLEMENTARY MATERIAL

See the supplementary material for details on how stoichiometric and gallium-rich conditions are found and defined. Supporting evidence is also presented regarding both the presence of a GaN interlayer in the gallium-rich structure and the indium incorporation in AlGaN layers grown by indium surfactant assisted epitaxy. Preliminary calculations supporting the strain-driven model of indium incorporation into low-temperature AlGaN grown by indium surfactant assisted epitaxy are also discussed.

ACKNOWLEDGMENTS

We acknowledge support from the National Science Foundation (NSF). A.S. and B.D. were supported by the NSF (Award No. ECCS-1607173). T.N., Y.C., and O.M. acknowledge partial support from NSF No. DMR-1610893. All STEM imaging and analyses were performed at the Electron Microscopy Facility at the Birck Nanotechnology Center, Purdue University.

DATA AVAILABILITY

The data that support the findings of this study are available within the article and its supplementary material.

REFERENCES

[1]M. Beeler, E. Trichas, and E. Monroy, Semicond. Sci. Technol. **28**, 074022 (2013).
[2]S. Nakamura, M. Senoh, S. Nagahama, N. Iwasa, T. Yamada, T. Matsushita, H. Kiyoku, and Y. Sugimoto, Jpn. J. Appl. Phys. **35**, L74 (1996).
[3]Y. Taniyasu, M. Kasu, and T. Makimoto, Nature **441**, 325 (2006).
[4]Y. Narukawa, Y. Kawakami, M. Funato, S. Fujita, S. Fujita, and S. Nakamura, Appl. Phys. Lett. **70**, 981 (1997).
[5]T. Nguyen, M. Shirazi-Hosseini-Dokht, Y. Cao, R. E. Diaz, G. C. Gardner, M. J. Manfra, and O. Malis, Physica Status Solidi A **215**, 1700828 (2018).
[6]C. B. Lim, M. Beeler, A. Ajay, J. Lähnemann, E. Bellet-Amalric, C. Bougerol, and E. Monroy, J. Appl. Phys. **118**, 014309 (2015).
[7]C. B. Lim, A. Ajay, C. Bougerol, B. Haas, J. Schörmann, M. Beeler, J. Lähnemann, M. Eickhoff, and E. Monroy, Nanotechnology **26**, 435201 (2015).
[8]T. Kotani, M. Arita, and Y. Arakawa, Appl. Phys. Lett. **105**, 261108 (2014).
[9]C. B. Lim, M. Beeler, A. Ajay, J. Lähnemann, E. Bellet-Amalric, C. Bougerol, J. Schörmann, M. Eickhoff, and E. Monroy, Jpn. J. Appl. Phys. **55**, 05FG05 (2016).
[10]J. S. Speck and S. F. Chichibu, MRS Bull. **34**, 304 (2009).
[11]M. Leroux, N. Grandjean, M. Laügt, J. Massies, B. Gil, P. Lefebvre, and P. Bigenwald, Phys. Rev. B **58**, R13371 (1998).
[12]S. R. Lee, D. D. Koleske, K. C. Cross, J. A. Floro, K. E. Waldrip, A. T. Wise, and S. Mahajan, Appl. Phys. Lett. **85**, 6164 (2004).
[13]M. Shirazi-HD, R. E. Diaz, T. Nguyen, J. Jian, G. C. Gardner, H. Wang, M. J. Manfra, and O. Malis, J. Appl. Phys. **123**, 161581 (2018).
[14]J. Smalc-Koziorowska, M. Sawicka, T. Remmele, C. Skierbiszewski, I. Grzegory, and M. Albrecht, Appl. Phys. Lett. **99**, 061901 (2011).
[15]M. Sawicka, C. Chèze, H. Turski, J. Smalc-Koziorowska, M. Kryśko, S. Kret, T. Remmele, M. Albrecht, G. Cywiński, I. Grzegory, and C. Skierbiszewski, J. Cryst. Growth **377**, 184 (2013).
[16]I. Bryan, Z. Bryan, S. Mita, A. Rice, L. Hussey, C. Shelton, J. Tweedie, J.-P. Maria, R. Collazo, and Z. Sitar, J. Cryst. Growth **451**, 65 (2016).
[17]M. N. Fireman, B. Bonef, E. C. Young, N. Nookala, M. A. Belkin, and J. S. Speck, J. Appl. Phys. **122**, 075105 (2017).
[18]S. Birner, T. Zibold, T. Andlauer, T. Kubis, M. Sabathil, A. Trellakis, and P. Vogl, IEEE Trans. Electron Devices **54**, 2137 (2007).
[19]A. Senichev, B. Dzuba, T. Nguyen, Y. Cao, M. A. Capano, M. J. Manfra, and O. Malis, APL Mater. **7**, 121109 (2019).
[20]E. J. Tarsa, B. Heying, X. H. Wu, P. Fini, S. P. DenBaars, and J. S. Speck, J. Appl. Phys. **82**, 5472 (1997).
[21]P. Pramanik, S. Sen, C. Singha, A. S. Roy, A. Das, S. Sen, A. Bhattacharyya, D. Kumar, and D. V. Sridhara Rao, J. Cryst. Growth **439**, 60 (2016).
[22]T. M. Al Tahtamouni, A. Sedhain, J. Y. Lin, and H. X. Jiang, Appl. Phys. Lett. **92**, 092105 (2008).
[23]Z. Liang, X. Zhang, Q. Dai, H. Luan, J. Zhao, Z. Wu, G. Hu, and Y. Cui, J. Mater. Sci. Mater. Electron. **28**, 15217 (2017).
[24]E. Monroy, B. Daudin, E. Bellet-Amalric, N. Gogneau, D. Jalabert, F. Enjalbert, J. Brault, J. Barjon, and L. S. Dang, J. Appl. Phys. **93**, 1550 (2003).
[25]Q. Dai, X. Zhang, Z. Liang, G. Yang, Z. Wu, S. Chen, J. Zhao, C. Meng, J. Wang, and Y. Cui, Opt. Mater. Express **8**, 24 (2018).
[26]M. Sawicka, A. Feduniewicz-Żmuda, M. Kryśko, H. Turski, G. Muziol, M. Siekacz, P. Wolny, and C. Skierbiszewski, J. Cryst. Growth **459**, 129 (2017).
[27]C. S. Gallinat, G. Koblmüller, J. S. Brown, and J. S. Speck, J. Appl. Phys. **102**, 064907 (2007).
[28]M. Shirazi-HD, K. Turkmeneli, S. Liu, S. Dai, C. Edmunds, J. Shao, G. Gardner, D. N. Zakharov, M. J. Manfra, and O. Malis, Appl. Phys. Lett. **108**, 121108 (2016).
[29]H. Hirayama, Y. Aoyagi, and S. Tanaka, Mater. Res. Soc. Internet J. Nitride Semicond. Res. **4**, 852 (1999).
[30]T. Markurt, L. Lymperakis, J. Neugebauer, P. Drechsel, P. Stauss, T. Schulz, T. Remmele, V. Grillo, E. Rotunno, and M. Albrecht, Phys. Rev. Lett. **110**, 036103 (2013).
[31]S. Fritze, A. Dadgar, H. Witte, M. Bügler, A. Rohrbeck, J. Bläsing, A. Hoffmann, and A. Krost, Appl. Phys. Lett. **100**, 122104 (2012).
[32]M. Siekacz, G. Muziol, M. Hajdel, M. Żak, K. Nowakowski-Szkudlarek, H. Turski, M. Sawicka, P. Wolny, A. Feduniewicz-Żmuda, S. Stanczyk, J. Moneta, and C. Skierbiszewski, Opt. Express **27**, 5784 (2019).
[33]Z. H. Feng, S. J. Cai, K. J. Chen, and K. M. Lau, Appl. Phys. Lett. **88**, 122113 (2006).
[34]E. Monroy, B. Daudin, N. Gogneau, E. Bellet-Amalric, D. Jalabert, and J. Brault, Phys. Stat. Solidi. B **234**, 726–729 (2002).
[35]E. Dimakis, E. Iliopoulos, K. Tsagaraki, Th. Kehagias, Ph. Komninou, and A. Georgakilas, J. Appl. Phys. **97**, 113520 (2005).
[36]J. E. Northrup and J. Neugebauer, Phys. Rev. B **60**, R8473 (1999).